JOURNAL OF PROPULSION AND POWER
Vol. 17, No. 5, September–October 2001

Magnetohydrodynamics Energy Bypass Scramjet Performance with Real Gas Effects

Chul Park*
Eloret Corporation, Sunnyvale, California 94087
Unmeel B. Mehta†
NASA Ames Research Center, Moffett Field, California 94035
and
David W. Bogdanoff‡
Eloret Corporation, Sunnyvale, California 94087

The theoretical performance of a scramjet propulsion system incorporating a magnetohydrodynamic (MHD) energy bypass scheme is calculated. The one-dimensional analysis developed earlier, in which the theoretical performance is calculated neglecting skin friction and using a sudden-freezing approximation for the nozzle flow, is modified to incorporate the method of Van Driest for turbulent skin friction and a finite-rate chemistry calculation in the nozzle. Unlike in the earlier design, in which four ramp compressions occurred in the pitch plane, in the present design the first two ramp compressions occur in the pitch plane, and the next two compressions occur in the yaw plane. The results for the simplified design of a spaceliner show that 1) skin friction substantially reduces thrust and specific impulse and 2) the specific impulse of the MHD-bypass system is still better than the non-MHD system and typical rocket over a range of flight speeds and design parameters. Results suggest that the energy management with MHD principles offers the possibility of improving the performance of the scramjet for the spaceliner application and for the globecruiser application. The technical issues needing further studies are identified.

Nomenclature

B	=	magnetic field strength, T
E	=	electric field strength, V/m
H	=	height of vehicle, m
h	=	reactor entrance height/width, m
M_c	=	combustor entrance Mach number
P	=	pitch (Fig. 3)
T	=	temperature, K
u	=	axial velocity, m/s
V	=	flight velocity, m/s
x	=	axial distance, m
y	=	lateral distance, m
α_1	=	load factor (E_y/uB) for generator
α_2	=	load factor (E_y/uB) for accelerator
δ	=	boundary-layer momentum thickness, m
θ	=	ramp angle, deg

Introduction

IN a scramjet propulsion system, one well-known difficulty is that combustion is inefficient in the combustor when the Mach number of the airflow entering the combustor is high because of the poor mixing between fuel and air. In Refs. 1–3, it was noted that energy management with magnetohydrodynamic (MHD) techniques present a possible means for extending the flight Mach number envelope of conventional engines. This idea can also be used to improve the performance of the scramjet combustor by the use of the MHD principles.[4] In the proposal, the flow entering the combustor is to be decelerated by the use of an MHD generator. The electrical energy extracted from the MHD generator is expended to accelerate the flow by the use of an MHD accelerator after the combustion and before entering the nozzle expansion.

In Refs. 4 and 5, the theoretical performance of such an MHD-energy bypass scramjet propulsion system is calculated under several simplifying assumptions. The most important of those assumptions are that 1) the flow is inviscid and, therefore, no friction drag is produced, 2) the chemical reactions in the expanding nozzle undergo freezing suddenly, and 3) inlet compression occurs by four ramp compressions in the pitch plane. The calculation presents an envelope of specific impulse values attainable with such a system under these assumptions and compares it with those for a non-MHD scramjet system. The comparison shows that, in the flight speed range from about 3.4 to 4 km/s, the MHD-bypass system produces specific impulses higher than the non-MHD system and a typical rocket.

In the present work, the earlier method of performance calculation is improved. The flow is taken to be viscous, and the chemical reactions occur at a finite rate. The first two ramp compressions occur in the pitch plane, but the next two ramp compressions occur in the yaw plane. Other assumptions used in Ref. 4, such as ideal one-dimensional performance of the MHD devices, are retained in the present work.

The results show that finite-rate chemistry produces nearly the same results as the sudden-freezing approximation, the new geometry produces generally larger specific impulse, but the friction substantially reduces specific impulse. However, compared with the non-MHD system, the MHD-bypass system is still superior in a speed range from 3.0 to 3.9 km/s under certain restrictions on the geometry. The areas needing further research and development are identified.

Method

Two-Plane Four-Ramp Design

In an idealized scramjet system, the compression of the airflow entering the combustion chamber is achieved through the use of

Received 26 September 2000; revision received 29 March 2001; accepted for publication 19 May 2001.

*Senior Research Scientist, Mail Stop 229-1, Space Technology Division, NASA Ames Research Center, Moffett Field, CA 94035; cpark@mail.arc.nasa.gov. Fellow AIAA.

†Division Scientist, Space Technology Division, Mail Stop 229-3; umehta@mail.arc.nasa.gov. Associate Fellow AIAA.

‡Senior Research Scientist; Mail Stop 230-2, Reacting Flow Environments Branch, NASA Ames Research Center, Moffett Field, CA 94035; dbogdanoff@mail.arc.nasa.gov. Associate Fellow AIAA.

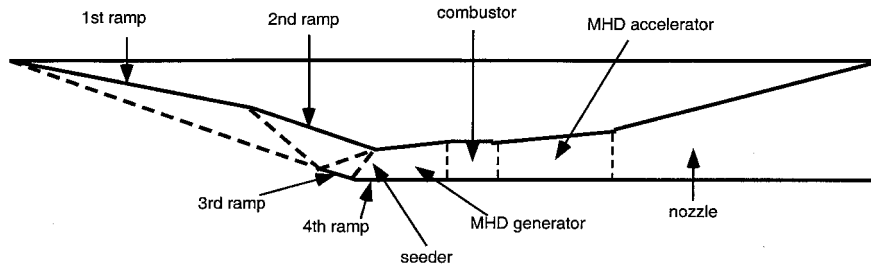

Fig. 1 Quasi-one-dimensional single-plane four-ramp compression inlet system.[4]

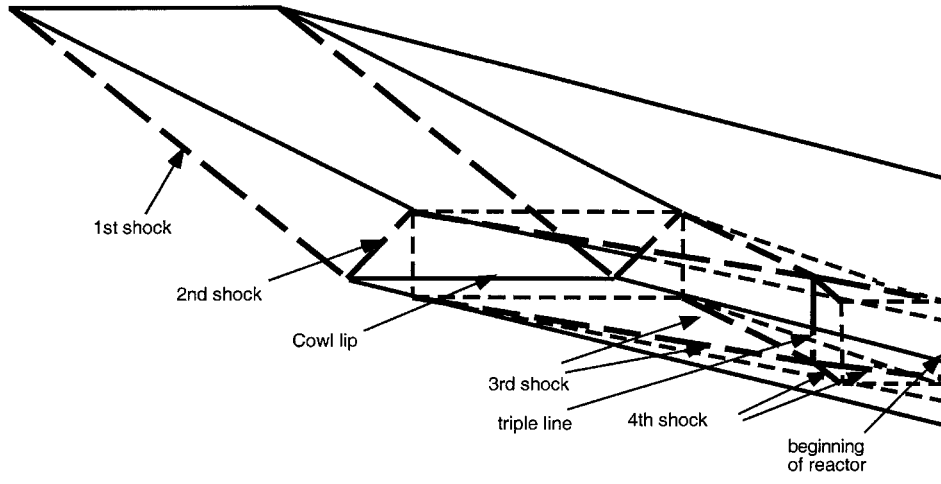

Fig. 2 Schematic of two-plane four-ramp compression inlet system with shock patterns.

a curved ramp, which compresses air through a nearly isentropic process to an angle typically of about 15 deg. At the end of this compression, the flow is turned abruptly in the inlet of the engine so that the flow becomes approximately parallel to the oncoming freestream. The flow then enters an isolator wherein the flow passes through multiple weak shock waves. The isolator isolates inlet operation from the effects of combustion-induced disturbances. The flow is generally three dimensional. The combustor following the isolator is usually relatively long because a long distance is needed for the flow to complete combustion at high supersonic or hypersonic speeds.

In Ref. 4, this complex compression process is approximately represented by a simple four-ramp system. In that representation, the flow makes four turns of a same specified angle within the pitch plane, as shown schematically in Fig. 1. This design will be referred to hereafter as single-plane four-ramp compression design. In this design, the flow entering the reactor (MHD generator plus combustor plus MHD accelerator) has a laterally elongated cross section: The width spans the entire vehicle and the height is only about few centimeters. In an inviscid calculation, this elongated cross-section had no consequences.

One drawback of the single-plane, four-ramp compression design is that it becomes difficult to construct the MHD devices with elongated (high aspect ratio) rectangular cross sections. Both the electrical and magnetic fields will be easier to produce and have reduced losses if the MHD devices have a square cross section. Another drawback is that the skin friction inside such as high aspect ratio channel becomes large because the geometry produces a large wetted-surface area. To reduce the skin friction to the minimum, the wetted area inside the reactor must be kept to the minimum. The minimum wetted area is obtainable with a square cross section. When other design factors are considered, a square cross section could be nonoptimum or inappropriate.

As in the single-plane four-ramp design, all turn angles are assumed to be equal. The consequences of deviating from this assumption are discussed later. The first two turns are made within the pitch plane, but the next two turns are made within the yaw plane, as shown schematically in Figs. 2 and 3. The lengths of ramps are specified in this model such that, at the end of the four-step compression, the cross section of the flow path is a square. The dimensions of the design are uniquely determined by specifying the common ramp angle θ and the height of the vehicle H (see Fig. 3). The overall length of the vehicle is fixed at 46 m. Of particular interest is the pitch, P and the width and height of the reactor at its entrance h (see Fig. 3). This design is termed two-plane four-ramp compression design. The scramjet vehicle employing such a four-ramp system is shown schematically in Fig. 4. Several of those engine units are ganged laterally.

In Fig. 5, the reactor is shown schematically for both non-MHD and MHD-bypass systems. For a non-MHD system, the reactor consists of an isolator, a fuel injector, and a combustor. For an MHD-energy bypass system, the isolator must function also as a seeder and an MHD power generator. A fuel injector must follow the MHD generator. The combustor, connected to the fuel injector, must function also as an MHD accelerator. The lengths of these components are chosen arbitrarily as shown in Fig. 5 for the present work. The cross section is assumed to be always a square. The dimensions of the square vary slightly for the MHD case because of the increase in entropy due to joule heating and because of the flow acceleration.

Inviscid Calculation Along Flow Path

As in Ref. 4, the flow properties are assumed to be in equilibrium up until the point in the nozzle at which chemical freezing takes place. In the MHD generator and accelerator, the flow is assumed to be uniform across the cross section. The ideal one-dimensional MHD equations, given in Ref. 4, are assumed to be valid. The parameter dictating the design of the MHD devices is the load factor $\alpha = E_y/uB$. This parameter, the dimension of the entrance of the MHD device (h for the generator and the corresponding dimension

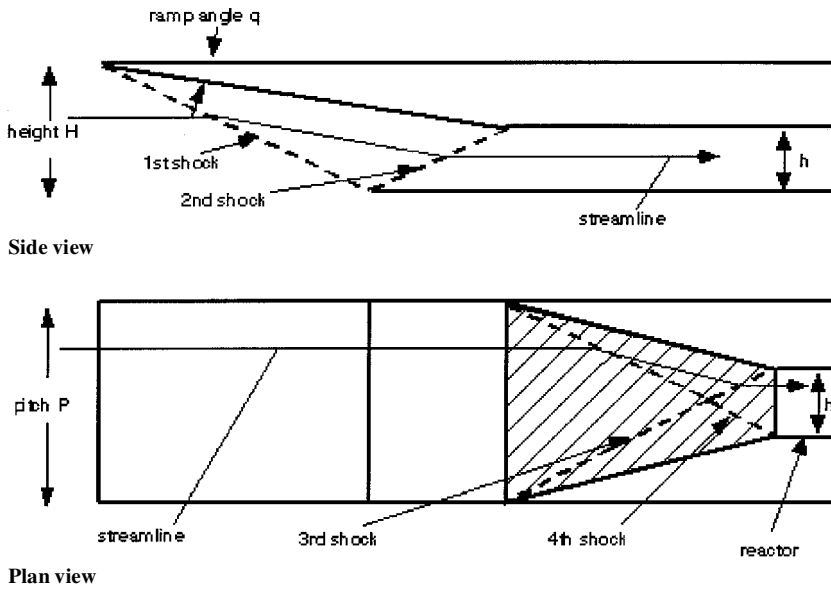

Fig. 3 Flow path in the two-plane four-ramp compression inlet system.

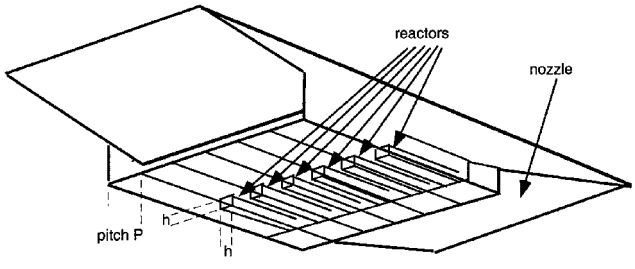

Fig. 4 Schematic view of a scramjet vehicle employing two-plane four-ramp inlet system.

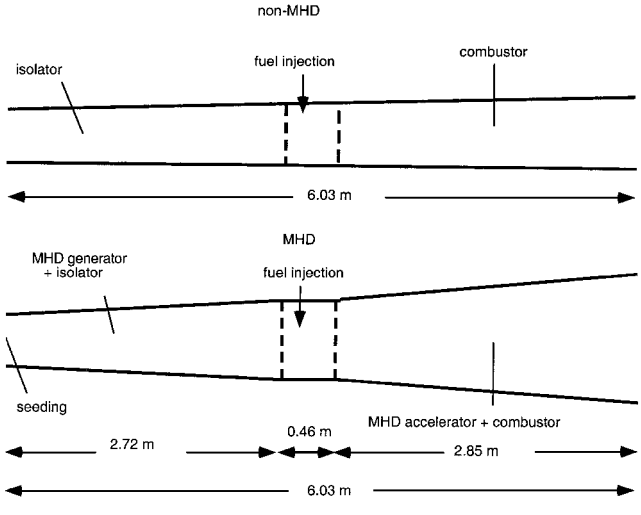

Fig. 5 Schematic of the reactor.

for the accelerator, see Fig. 3), and the requirement that the MHD action be completed at the end of the given length of the MHD device completely specify the design of the MHD devices including the magnetic field strength B, the electrical field strength in the lateral and axial directions, E_y and E_x, the electrical current, and the Hall parameter.

At the end of the fourth compression, seeding is assumed to occur. Liquid potassium or cesium is assumed to be injected into the flow instantly without causing shock waves or viscous dissipation. The flow exiting from the MHD generator enters the combustion chamber. Here, gaseous hydrogen fuel is assumed to be mixed instantly without causing any shock waves or viscous dissipation.

In Ref. 4, the mass fraction of the seed substance was varied. The optimum values of mass fraction were found to be about 0.001 for potassium and 0.003 for cesium by mass. These values are assumed in the present work throughout. The method of fuel injection is described in Ref. 4.

To calculate the inviscid flow properties, the expansion following the MHD accelerator is assumed to occur with a linearly increasing cross-sectional area. The rate of increase of the cross-sectional area is chosen so that, at the end of the expansion, the height of the nozzle equals the height of the vehicle, as indicated in Fig. 4.

In Ref. 4, the flow properties are calculated for the expansion region using a sudden-freezing approximation. In the present work, this is replaced by a finite-rate kinetic calculation. The chemical species considered are O, N, H, O_2, N_2, H_2, NO, OH, H_2O, and a seed substance, its ions, and electrons. The seed substance is potassium K or cesium Cs. The forward (endothermic) reaction rates [cm^3/(mol-s)] are expressed as

$$k = AT^n \exp(-Tr/T)$$

The parameters A, n, and Tr are obtained from Refs. 6–9. They are summarized in Table 1.

Skin Friction

The boundary-layer flow along the wall in the flow path is assumed to be fully turbulent. Van Driest equations[10] (see Ref. 11) for fully turbulent flow over a flat plate are used to calculate the skin friction. These equations yield the skin friction over a flat plate between the given distances x_1 and x_2 away from the sharp leading edge. At x_1, the equations yield also the boundary-layer momentum thickness δ_1. The thickness δ_1 can be used interchangeably to denote the distance x_1. This relationship between δ_1, rather than x_1, and skin friction is made into a routine in the present work.

This routine is then used in calculating the friction over a curved surface or a flat surface with varying flow conditions. The surface is divided first into small segments of length $\Delta x = x_2 - x_1 = 0.05$ m. At the apex of the vehicle or the leading edge of the cowl, that is, the second ramp (see Fig. 3), δ is zero. Over each Δx, the flow properties at the edge of the boundary layer are assumed to be unchanged. Then, using the routine, the friction over that segment is calculated. The calculation yields the δ value at the exit of this segment, δ_2. This δ_2 value is used in the calculation for the next segment, and so on.

Table 1 Reaction rates used where *M* is the third body

M	A,cm^3/(mol-s)	n	Tr	Reference
	$H_2 + M \longrightarrow H + H + M$			
O	2.940*e* 18	−1.0	52,500	Baulch et al.[7]
N	2.940*e* 18	−1.0	52,500	Baulch et al.[7]
H	2.940*e* 18	−1.0	52,500	Baulch et al.[7]
K/Cs	2.940*e* 18	−1.0	52,500	Baulch et al.[7]
O_2	2.940*e* 18	−1.0	52,500	Baulch et al.[7]
N_2	2.940*e* 18	−1.0	52,500	Baulch et al.[7]
H_2	7.350*e* 18	−1.0	52,500	Baulch et al.[7]
NO	2.940*e* 18	−1.0	52,500	Baulch et al.[7]
OH	2.940*e* 18	−1.0	52,500	Baulch et al.[7]
H_2O	4.780*e* 19	−1.0	52,500	Ref. 8
K^+/Cs^+	2.940*e* 18	−1.0	52,500	Baulch et al.[7]
	$O_2 + M \longrightarrow O + O + M$			
O	5.090*e* 18	−1.1	59,360	Park[6]
N	5.090*e* 18	−1.1	59,360	Park[6]
H	5.090*e* 18	−1.1	59,360	Park[6]
K/Cs	5.090*e* 18	−1.1	59,360	Park[6]
O_2	5.090*e* 18	−1.1	59,360	Park[6]
N_2	5.090*e* 18	−1.1	59,360	Park[6]
H_2	2.000*e* 18	−1.1	59,360	Park[6]
NO	1.270*e* 19	−1.1	59,360	Park[6]
OH	5.090*e* 18	−1.1	59,360	Park[6]
H_2O	8.270*e* 19	−1.1	59,360	Park[6]
K^+/Cs^+	5.090*e* 18	−1.1	59,360	Park[6]
	$OH + M \longrightarrow +H + M$			
O	2.400*e* 13	0.3	5,000	Baulch et al.[7]
N	2.400*e* 13	0.3	5,000	Baulch et al.[7]
H	2.400*e* 13	0.3	5,000	Baulch et al.[7]
K/Cs	2.400*e* 13	0.3	5,000	Baulch et al.[7]
O_2	2.400*e* 13	0.3	5,000	Baulch et al.[7]
N_2	2.400*e* 13	0.3	5,000	Baulch et al.[7]
H_2	6.000*e* 13	0.3	5,000	Baulch et al.[7]
NO	2.400*e* 13	0.3	5,000	Baulch et al.[7]
OH	2.400*e* 13	0.3	5,000	Baulch et al.[7]
H_2O	3.900*e* 14	0.3	5,000	Baulch et al.[7]
K^+/Cs^+	2.400*e* 13	0.3	5,000	Baulch et al.[7]
	$H_2O + M \longrightarrow OH + H + M$			
O	1.060*e* 25	−2.5	61,000	Baulch et al.[7]
N	1.060*e* 25	−2.5	61,000	Baulch et al.[7]
H	1.060*e* 25	−2.5	61,000	Baulch et al.[7]
K/Cs	1.060*e* 25	−2.5	61,000	Baulch et al.[7]
O_2	1.060*e* 25	−2.5	61,000	Baulch et al.[7]
N_2	1.060*e* 25	−2.5	61,000	Baulch et al.[7]
H_2	2.650*e* 25	−2.5	61,000	Baulch et al.[7]
NO	1.060*e* 25	−2.5	61,000	Baulch et al.[7]
OH	1.060*e* 25	−2.5	61,000	Baulch et al.[7]
H_2O	1.720*e* 26	−2.5	61,000	Baulch et al.[7]
K^+/Cs^+	1.060*e* 25	−2.5	61,000	Baulch et al.[7]
	$K + e^- \longrightarrow K^+ + e^- + e^-$			
	3.900*e* 33	−3.78	45,180	Park[6]
	$Cs + e^- \longrightarrow Cs^+ + e^- + e^-$			
	3.900*e* 33	−3.78	45,180	Park[6]
	$N_2 + O \longrightarrow NO + N$			
	5.690*e* 12	0.42	42,938	Bose and Candler[9]
	$O + NO \longrightarrow N + O_2$			
	2.360*e* 9	1.00	19,220	Park[6]
	$H_2O + H \longrightarrow H_2 + OH$			
	2.760*e* 10	1.12	10,250	Baulch et al.[7]
	$H_2 + O \longrightarrow H + OH$			
	5.060*e* 4	2.67	3,166	Baulch et al.[7]
	$O_2 + H \longrightarrow OH + O$			
	1.910*e* 14	0	8,273	Baulch et al.[7]

In the region of the third ramp (the hatched area in Fig. 3b), the streamline starting at different lateral positions encounter the third and the fourth shock at different locations. For this region, the friction over a unit width is first calculated along five different streamlines and is integrated to evaluate the total friction over these panels using Simpson's rule. Calculations showed that five streamlines lead to solutions that are accurate to within 0.1% compared to those solutions with nine streamlines.

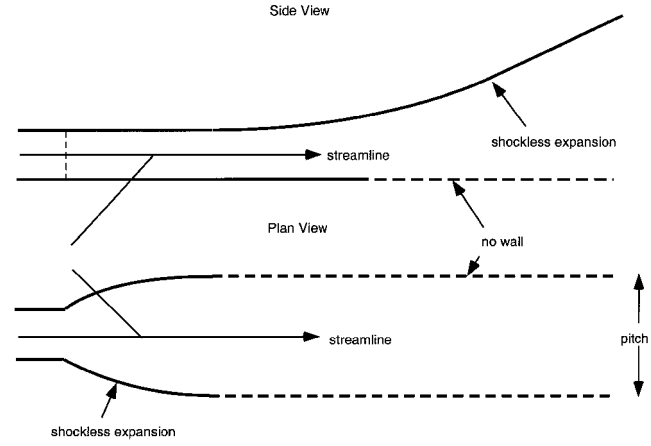

Fig. 6 Schematic of the transition from the MHD accelerator to one-sided expansion.

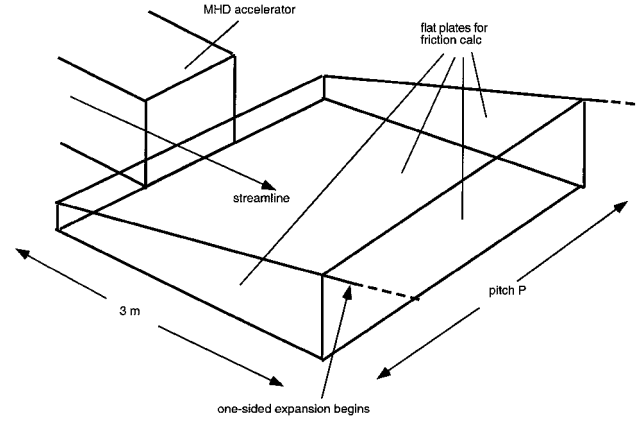

Fig. 7 Flat plates assumed for friction calculation of the contoured expansion region.

For the contoured portion of the expansion, shown schematically in Fig. 6, accurate calculation of skin friction is difficult because the contours are unknown. Here, skin friction is assumed to be that of the four flat plates shown in Fig. 7. The lengths of these flat plates are arbitrarily assumed to be 3 m as shown. The inaccuracies in computing the skin-friction drag do not impact the conclusion regarding which design, MHD or non-MHD, generates higher specific impulse because drag in both cases is computed in the same manner.

Highest Specific Impulse

The combustor entrance Mach number M_c is varied as 1.5, 2.0, and 2.5, which are within the realistic range of possibilities for a scramjet combustor. The vehicle height H is varied as 3.5, 4, 4.5, 5, and 5.5 m, although most of the results are for 3.5 m. The load factor pair, α_1–α_2', is varied as 0.95–1/0.95, 0.90–1/0.90, and 0.80–1/0.80. The fuel equivalence ratio is kept at unity for all cases, and the flight dynamic pressure is kept at 1 atm.

For a flight speed V, the combustor entrance Mach number M_c, the vehicle height H, and the seed substance and seed mass fraction chosen, one can vary the ramp angle θ arbitrarily. The resulting specific impulse value is a function of the ramp angle. Calculation is performed at an interval in θ of 0.1 deg to first produce a table of specific impulse vs θ. The ramp angle giving the highest specific impulse is chosen from this table as the optimum ramp angle for that condition.

The thrust is calculated as the difference between the outgoing (at the tail of the vehicle) and incoming (at the nose of the vehicle) momentum, $(p + \rho u^2) \times$ area, minus the friction drag. Specific impulse is calculated by dividing this thrust by the sum of the flow rates of the fuel and the seed material.

Results

General Features of Solutions

In Fig. 8, the specific impulses obtained by the present method are compared with those obtained by the sudden-freezing approximation used in Refs. 4 and 5, for the single-plane four-ramp compression system considered therein. The combustor entrance Mach number M_c was 2 for this case. Skin-friction drag is not included in this comparison. As seen in Fig. 8, there is only a small difference between the kinetic and sudden-freezing calculations.

In Fig. 9, the optimum vehicle geometry is compared between typical MHD and non-MHD cases with friction and with finite-rate chemistry in the nozzle. For this case, $V = 3.75$ km/s, α_1 and α_2 are 0.95 and 1/0.95, $M_c = 1.5$, and $H = 7$ m. As indicated, the optimum angle of the ramps for the MHD and the non-MHD cases are $\theta = 17.1$ and 22.1 deg, respectively. As has been pointed out in Ref. 4, this difference in the optimum θ occurs because of the constraint on Mach number M_c.

The pressure distribution along the flow path for these two vehicles is compared in Fig. 10. As shown here, because of the large θ, the non-MHD vehicle is subject to a higher pressure in the inlet region than the MHD vehicle. This causes larger form drag for the non-MHD vehicle. The specific impulses for these two cases are 650 s for the MHD vehicle and 345 s for the non-MHD vehicle.

Figures 11a and 11b show for the two vehicles the friction drag per meter of the vehicle width. Because θ is different between the two vehicles, the friction drag values are slightly different on the three ramps. The friction drag for these ramps is slightly larger for the MHD case because the MHD case produces longer ramps. The sum of the drags by the MHD generator, fuel injector, and the MHD accelerator for the MHD vehicle, shown in Fig. 11b, is lower than the sum of the drags by the isolator and the combustor for the non-MHD vehicle shown in Fig. 11a.

The details of a typical solution for a two-plane four-ramp compression design are given in Table 2. The highlights of this solution

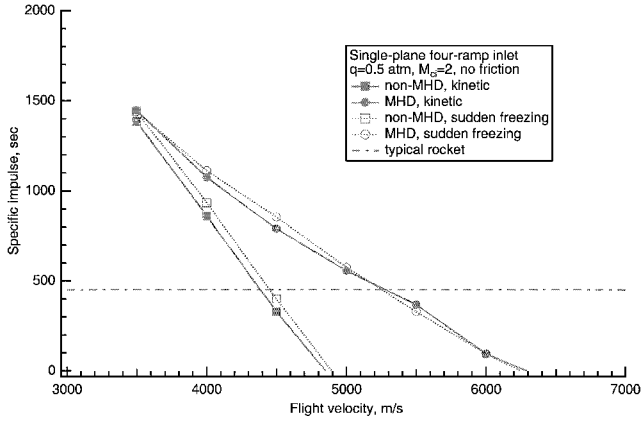

Fig. 8 Comparison of the specific impulse obtained by kinetic calculation and that with the sudden-freezing calculation; $\alpha_1 = 0.95$, $\alpha_2 = 1/0.95$, and potassium seed.

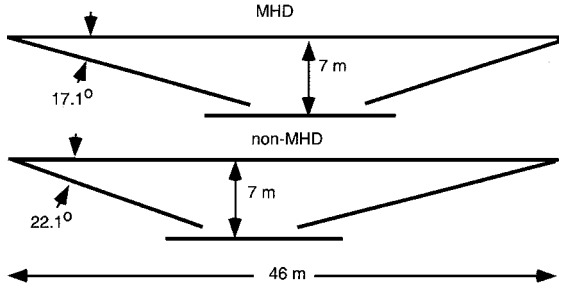

Fig. 9 Comparison of the optimum configuration between the MHD and the non-MHD vehicles: $V = 3.75$ km/s, $M_c = 1.5$, $H = 7$ m, $\alpha_1 = 0.95$, $\alpha_2 = 1/0.95$, and potassium seed.

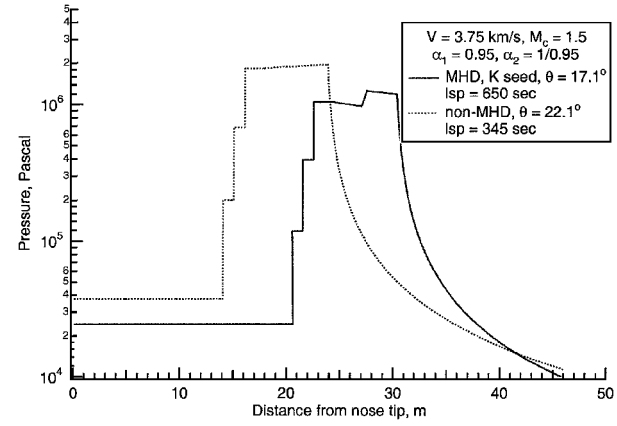

Fig. 10 Comparison of static pressure distribution over the MHD and the non-MHD vehicles with friction and finite-rate chemistry in the nozzle: $V = 3.75$ km/s, $M_c = 1.5$, $H = 7$ m, $\alpha_1 = 0.95$, and $\alpha_2 = 1/0.95$.

are that 1) the height is 7 m, the ramp angle is 17.1 deg, and the pitch is 2.82 m; 2) the vehicle produces 74.7 ton of thrust per 1 m of vehicle width and a specific impulse of 650 s (as opposed to 345 s for the non-MHD vehicle); 3) the load factors α_1 and α_2 are 0.95 and 1/0.95, respectively; 4) the magnetic fields required for the MHD generator and accelerator are 12.7 and 11.3 T, respectively; and 5) the maximum axial voltage gradient of 5260 V/m slightly exceeds the limiting value of 5000 V/m used in Ref. 4.

Parametric Study

In Fig. 12, the calculated specific impulse values for $M_c = 1.5$ are compared between the MHD case with potassium seeding and cesium seeding and with $\alpha_1 = 0.95$ and $\alpha_2 = 1/0.95$, the non-MHD case, and a typical rocket (with specific impulse of 450 s). The plotted with-friction values are obtained by choosing the ramp angle θ that maximizes the specific impulse while including friction in the thrust calculation. That is, the design is optimized including friction. The without-friction values plotted are obtained by removing friction from the thrust calculation for the same vehicle at the same flight condition. The without-friction values are, therefore, not of the optimized vehicles.

As seen in Fig. 12, the skin friction for fully turbulent flow greatly reduces the specific impulse. The two MHD cases produce higher specific impulses than the non-MHD case at flight speed higher than 3000 m/s. Potassium seeding gives about the same specific impulse as cesium seeding. Compared with the single-plane four-ramp results shown in Fig. 8, the present results show higher specific impulses when friction is ignored (without-friction values). This is a result of the gradual expansion in the nozzle mentioned earlier.

The effect of changing the combustor entrance Mach number M_c on specific impulse is studied in Fig. 13. As seen here, the case of $M_c = 1.5$ with MHD yields higher specific impulses than the non-MHD case at flight speeds above 3000 m/s. As M_c increases from 1.5 to 2.0 to 2.5, the advantage of MHD becomes smaller. The effect of the load factors α_1 and α_2 on specific impulse is studied in Figs. 14a–14c. Specific impulse deteriorates with α_1 and α_2 deviating further away from unity.

The impact of varying vehicle height H on specific impulse is shown in Fig. 15 for $V = 3.75$ km/s and $M_c = 1.5$. When H is increased, the specific impulse of the MHD-bypass vehicle is increased. The specific impulse for the non-MHD vehicle also increases slightly but at a slower rate. As a result, for this condition the advantage of the MHD-bypass system increases at large H.

The optimum geometry of the present two-plane four-ramp compression design is one in which the reactor is located relatively close to the leading edge, as shown in Fig. 9. The location of the reactor can be moved aft by increasing the ramp angle of the third and fourth ramps. Calculation was performed with the angle of the third (and fourth) ramp that is 0.5, 0.75, 1.5, 2, and 2.5 times the angle

Table 2 Summary of a typical solution

Parameter	Value
Freestream	
Flight speed	3.75 km/s
Flight dynamic pressure	1 atm (2116 psf) (1.014×10^5 Pa)
Mach number	11.81
Freestream temperature	250 K
Freestream density	1.441×10^{-2} kg/m^3
Freestream pressure	1.039×10^3 Pa
Number of ramps	4
Ramp angles	17.1 deg
Over first ramp	
Pressure	2.440×10^4 Pa
Temperature	1422 K
Velocity	3471 m/s
Mach number	4.581
Pitch	2.820 m
Over second ramp	
Pressure	1.181×10^5 Pa
Temperature	2219 K
Velocity	3157 m/s
Mach number	3.937
Over third ramp	
Pressure	3.924×10^5 Pa
Temperature	2865 K
Velocity	2810 m/s
Mach number	3.066
Over fourth ramp (=entrance to seeder)	
Pressure	1.035×10^6 Pa
Temperature	3370 K
Velocity	2820 m/s
Mach number	2.422
Capture air flow rate	378.3 kg/s
Enthalpy flow	2.755×10^9 W/m
Seeding	
Entrance height/width	64.85 cm
Overall inlet area ratio	46.93
Seeding material	Potassium
Seed mass fraction	10^{-3}
Seed flow rate	0.3783 kg/s
Pressure	1.038×10^6 Pa
Temperature	3371 K
Ionization mol fraction	4.294×10^{-5}
Electrical conductivity	32.42 mho/m
Entrance to MHD generator	
Height/width of channel	64.85 cm
Magnetic field	12.74 T
Hall parameter	3.402
Transverse voltage gradient	−29,400 V/m
Axial voltage gradient	5263 V/m
Voltage across electodes	19066 V
Current density	-5.017×10^4 A/m^2
Pressure	1.038×10^6 Pa
Temperature	3371 K
Velocity	2429 m/s
Mach number	2.418
Enthalpy flow	2.755×10^9 W/m
At exit of MHD generator	
Magnetic field	12.74 T
Hall parameter	3.647
Transverse voltage gradient	−18,290 V/m
Axial voltage gradient	3511 V/m
Voltage across electrodes	15572 V
Current density	-8.175×10^4 A/m^2
Height/width of channel	85.14 cm
Pressure	9.667×10^5 Pa
Temperature	3365 K
Velocity	1511 m/s
Mach number	1.505
Length of generator	2.721 m
Enthalpy flow	2.070×10^9 W/m
Power extracted	6.848×10^8 W/m
At entrance to combustor	
Equivalence ratio	1
Fuel flow rate	11.11 kg/s
Height/width of channel	85.14 cm
Pressure	9.667×10^5 Pa
Temperature	3365 K
Velocity	1511 m/s
Mach number	1.505
Fuel injector	
Fuel	Gaseous hydrogen
Total temperature	500 K
Total pressure	2×10^7 Pa
Nozzle exit velocity	2865 m/s
Nozzle exit static pressure	9.668×10^5 Pa
At exit of injector section	
Pressure	1.251×10^6 Pa
Temperature	3583 K
Velocity	1361 m/s
Mach number	1.147
Enthalpy flow	2.150×10^9 W/m
At entrance to MHD accelerator	
Magnetic field	11.28 T
Hall parameter	2.259
Transverse voltage gradient	30,990 V/m
Axial voltage gradient	1825 V/m
Voltage across electrodes	15071 V
Current density	2.898×10^4 A/m^2
Height/width of channel	93.27 cm
Pressure	1.251×10^6 Pa
Temperature	3583 K
Velocity	1361 m/s
Mach number	1.147
Ionization fraction	5.583×10^{-5}
Electrical conductivity	35.87 mho/m
Enthalpy flow	2.120×10^9 W/m
At exit of MHD accelerator (=entrance to nozzle)	
Magnetic field	11.28 T
Hall parameter	2.379
Transverse voltage gradient	31,470 V/m
Axial voltage gradient	3307 V/m
Voltage across electrodes	20,300 V
Current density	5.022×10^4 A/m^2
Height/width of channel	72.98 cm
Pressure	1.185×10^6 Pa
Temperature	3574 K
Velocity	2342 m/s
Mach number	1.976
Length of accelerator	2.846 m
Enthalpy flow	2.819×10^9 W/m
Power consumed	6.848×10^8 W/m
At nozzle exit	
Area ratio	36.5
Pressure	9.763×10^3 Pa
Temperature	1943 K
Velocity	3872 m/s
Enthalpy flow	2.843×10^9 W/m
Mach number	4.168
Overall performance	
Energy bypass ratio	0.2820
Net thrust	7.322×10^4 N
Seed + fuel flow rate	11.50 kg/s
Specific impulse	649.5 s

of the first (and the second) ramp. The overall length of the vehicle is kept the same. In Fig. 16, the result of that calculation is shown. As Fig. 16 shows, increasing the third/fourth ramp affects the MHD and the non-MHD cases differently. The highest relative advantage of the MHD system is realized when the ratio is unity.

Discussion

In Ref. 4, a method was presented for assessing the theoretical performance of an MHD-energy bypass scramjet propulsion system

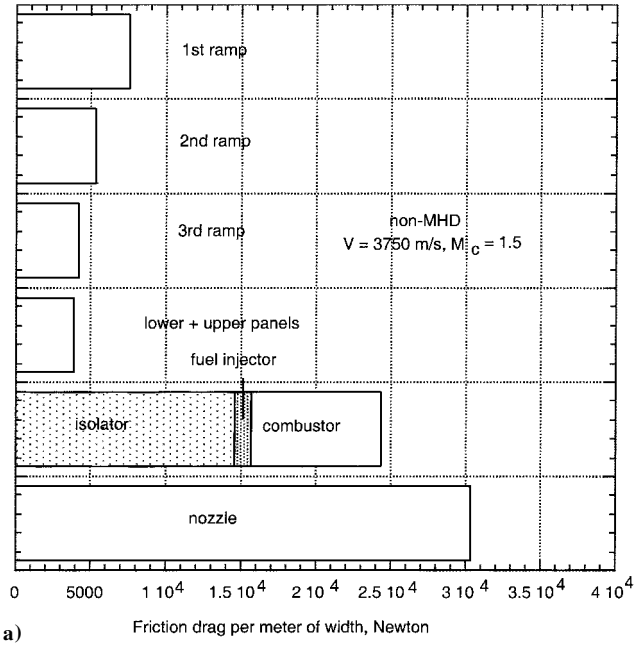

a)

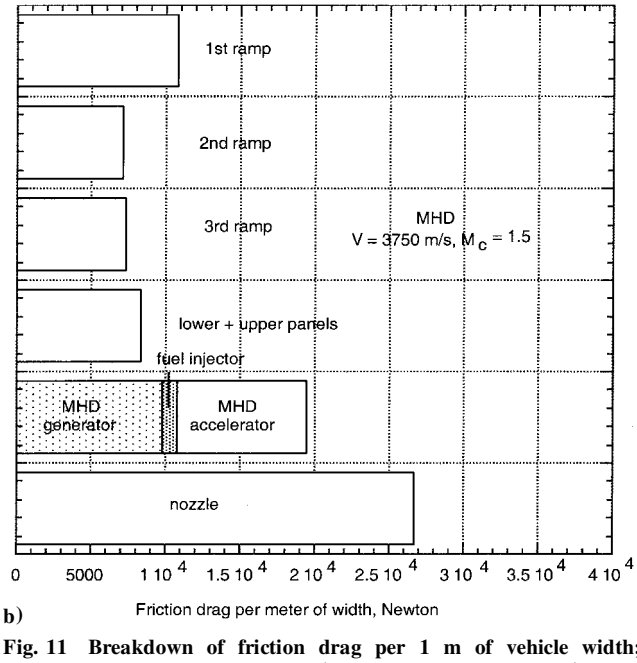

b)

Fig. 11 Breakdown of friction drag per 1 m of vehicle width; $V = 3750$ m/s, $M_c = 1.5$, $H = 7$ m: a) non-MHD vehicle, and b) MHD vehicle; $\alpha_1 = 0.95$, $\alpha_2 = 1/0.95$ and potassium seed.

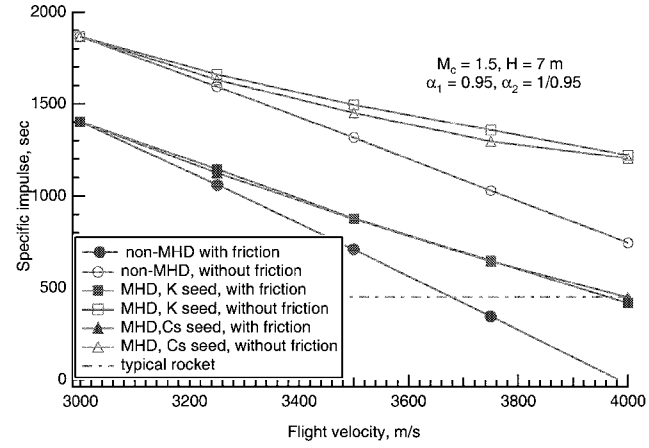

Fig. 12 Comparison of specific impulse with friction between the MHD case with potassium and cesium seed and the non-MHD case: $M_c = 1.5$, $\alpha_1 = 0.95$, $\alpha_2 = 1/0.95$ and $H = 7$ m.

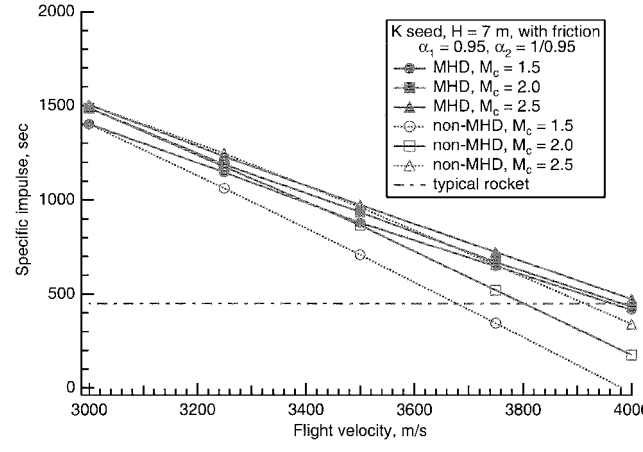

Fig. 13 Effect of combustor entrance Mach number M_c.

under several simplifying assumptions. In the present work, this method of performance calculation is improved by eliminating two key assumptions. The flow is taken to be viscous, and the chemical reactions occur at a finite rate. The improved method provides a more realistic assessment of this propulsion concept than the previous method did.

In the present work, the boundary layer in the flow path is assumed to be fully turbulent starting from the leading edge. The boundary layer over the first ramp and the second ramp are no doubt at least partly laminar. Consideration of laminar boundary layer over these two components will lower the skin-friction values for these two components. However, according to Figs. 11a and 11b, the contribution of these two components to the total drag is relatively small. The end result is that the inclusion of viscous friction lowers specific impulse substantially.

With the present design, the MHD-bypass system with $M_c = 1.5$ produces specific impulses that are better than those for the non-MHD scramjet system and for a typical rocket engine between the flight velocity of 3000 and 3900 m/s. Over a wide range of design parameters, the MHD-bypass system has an advantage over the non-MHD system. At the flight velocity of 3750 m/s with $M_c = 1.5$, the specific impulse for the MHD case exceeds that of the non-MHD case by about 305 s and that of the typical rocket by about 200 s. At this condition, the MHD-bypass system offers a clear advantage over the non-MHD case for the spaceliner application and the hypersonic cruiser application.

As already seen, the present two-plane four-ramp compression design is superior to the single-plane four-ramp design in Ref. 4. With the present design, performance is seen to be a complex function of the ramp angles and vehicle height. In reality, a portion of compression will be by an isentropic compression instead of shock compression. When isentropic compression is introduced into the design, performance will be an even more complex function of geometry. This offers hopes for further improving the performance of the MHD-energy bypass scramjet system.

In reality, it would probably be rather difficult to realize some of the assumptions made for the MHD system. First, the high computed results for magnetic field in the magnetic devices are currently not feasible for the spaceplane or globecruiser application, and lightweight MHD devices are not available for this application. Second, the power loss in the electrical system outside of the flow path and the reverse current in the boundary layer of the MHD devices are likely to lower the performance of the MHD devices. Additionally, the skin friction through the MHD devices may be larger than that for the non-MHD system, because the MHD devices have electrodes that produce effectively a rough surface. Third, equilibrium ionization with seeding requires temperatures greater than

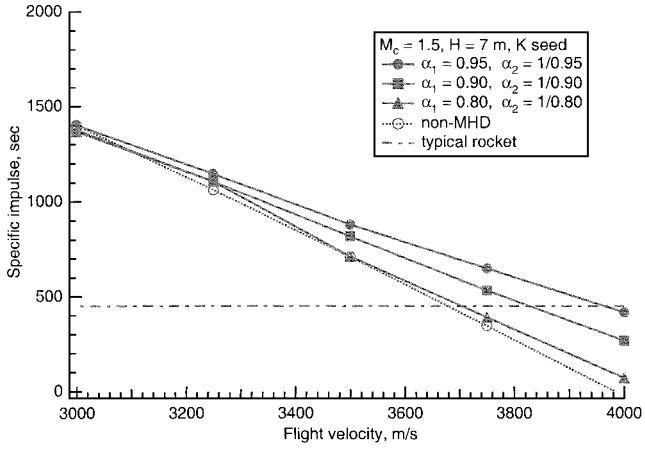

a) $M_c = 1.5$

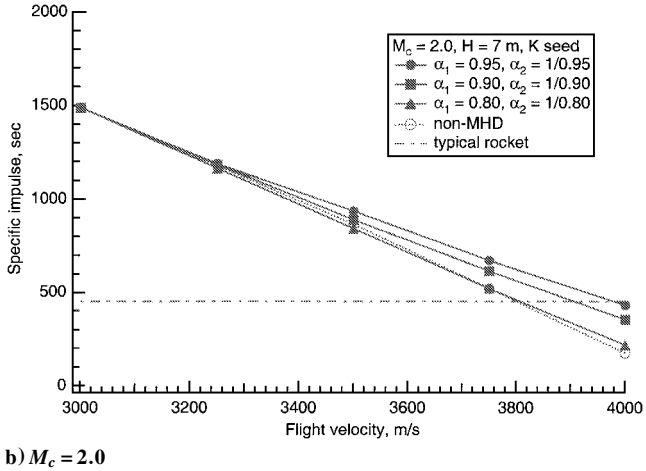

b) $M_c = 2.0$

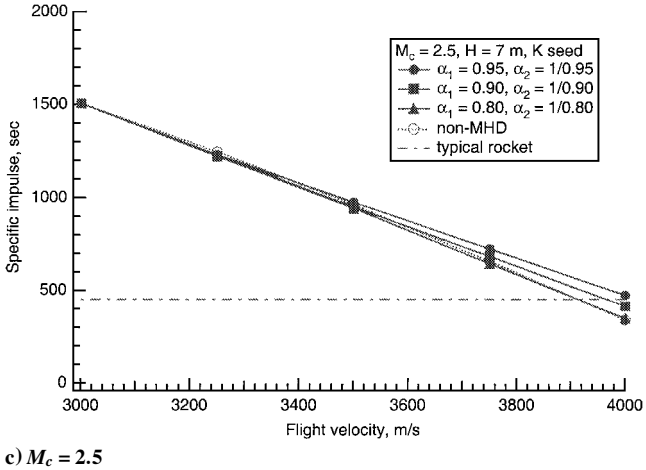

c) $M_c = 2.5$

Fig. 14 Effect of load factors α_1 and α_2 on specific impulse.

3000 deg K, presenting a challenge for designing an appropriate thermal management system made of lightweight materials that can withstand ultrahigh temperatures. Fourth, specific impulse of air-breathing hypersonic propulsion system is very sensitive to vehicle design and operation. Herein, a quasi-one-dimensional analysis is undertaken to investigate a small design space. Three-dimensional simulations are essential for fully accounting the effects of the electric and magnetic fields on the propulsive flowfield.

At moderate hypersonic flight Mach numbers, energy management using MHD devices allows operation of a scramjet engine as if it was operated at low hypersonic flight Mach numbers. A great deal of research and development would likely be necessary for the MHD devices to function as efficiently as assumed herein. The viability of energy management with MHD devices needs to be determined by conducting conceptual designs of realistic spaceliners

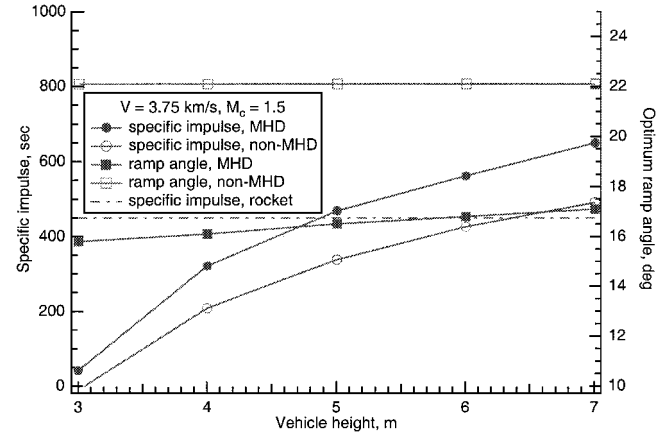

Fig. 15 Impact of vehicle height H on specific impulse.

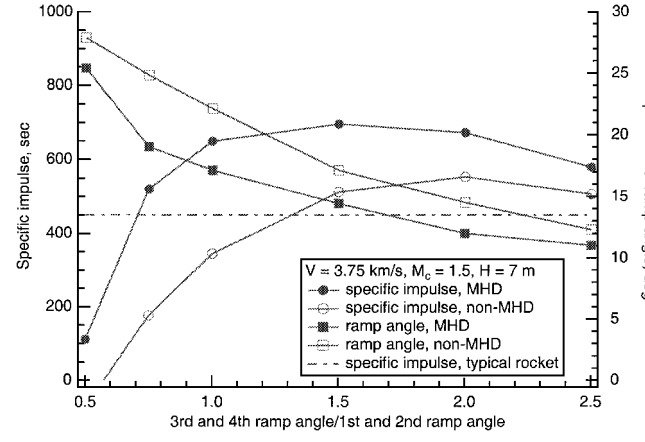

Fig. 16 Effect of changing the ratio of the third and fourth ramp angles to the first and second ramp angles.

and globecruisers and assessing vehicle performance using more sophisticated analysis methods.

Conclusions

Energy management with MHD offers the possibility of enhancing the performance of a scramjet engine. If the boundary layer of the flow in the propulsive flowpath for the MHD-energy bypass scramjet propulsion system is fully turbulent, the length of the reactor for the MHD-system (MHD generator plus fuel injector plus MHD accelerator) is the same as that of the non-MHD scramjet system, the combustor entrance Mach number is limited to 1.5, the height-to-length ratio of the vehicle is 7, and the MHD devices function as assumed, then the specific impulse of the MHD system is greater than that of the non-MHD system and a typical rocket within a speed range between 3000 and 3900 m/s. In this speed range, the MHD system offers an advantage over the non-MHD system and a typical rocket system for the spaceliner application. At the flight speed of 3750 m/s, the specific impulse of the MHD system is 305 and 200 s higher than that of the non-MHD system and that of a typical rocket system, respectively. At this speed, the MHD system offers an advantage over the non-MHD system for the globecruiser application. At flight speeds higher than 3900 m/s, the MHD system is still better than the non-MHD system, but the absolute value of specific impulse is below that of a typical rocket.

Specific impulse is a complex function of geometry; when geometry is varied and the analysis method is improved, further improvements in performance may be possible. A system analysis of a realistic spaceliner with MHD-bypass scramjet is recommended to assess the viability of this propulsion concept. Major research and technology issues are identified.

Acknowledgment

C. Park and D. W. Bogdanoff wish to acknowledge the support provided by NASA Ames Research Center through Contract NAS2-99092 to Eloret Corporation. The similar results presented in "Real-Gas Calculation of MHD-Bypass Scramjet Performance," by Park, Mehta, and Bogdanoff, AIAA Paper 2000-3702 (presented at the 36th AIAA/ASME/SAE/ASEE Joint Propulsion Conference and Exhibit, Huntsville, AL, 16–19 July 2000) for the scramjet vehicle employing two-plane four-ramp inlet system were found to contain computational errors. That paper should be disregarded.

References

[1]Novichov, N., "At Hypersonic Speeds (In the Large Scale Plan)," FASTC-ID(RS)T-0927-92, Foreign Aerospace Science and Technology Center, Wright–Patterson Air Force Base, Ohio, Jan. 1993; translated from *Ekho Planetary* (USSR), Vol. 42, No. 237, 1992, pp. 4–8.

[2]Gurijanov, E. P., and Harsha, P. T., "AJAX: New Directions in Hypersonic Technology," AIAA Paper 96-4609, Nov. 1996.

[3]Bityurin, V. A., Lineberry, J. T., Potebnia, V. G., Alferov, V. I., Kuranov, A. L., and Sheikin, E. G., "Assessment of Hypersonic MHD Concepts," AIAA Paper 97-2393, June 1997.

[4]Park, C., Bogdanoff, D. W., and Mehta, U. B, "Theoretical Performance of Frictionless Magnetohydrodynamic-Bypass Scramjet," *Journal of Propulsion and Power*, Vol. 17, No. 3, 2001, pp. 591–598.

[5]Chase, R. L., Mehta, U. B., Bogdanoff, D. W., Park, C., Lawrence, S., and Aftosmis, M., "Comments on an MHD Energy Bypass Engine Powered Spaceliner," AIAA Paper 99-4965, Nov. 1999.

[6]Park, C., *Nonequilibrium Hypersonic Aerothermodynamics*, Wiley, New York, 1990, p. 267.

[7]Baulch, D. L., Drysdale, D. D., and Horne, D. G., *Evaluated Kinetic Data for High Temperature Reactions*, CRC Press, Boca Raton, FL, 1972.

[8]"Hypersonic Combustion Kinetics," Status Report of the Rate Constant Committee, NASP High Speed Propulsion Technology Team, Dec. 1989.

[9]Bose, D., and Candler, G. V., "Thermal Rate Constants of the $N_2 + O \longrightarrow NO + N$ Reaction Using ab initio $^3A"$ and $^3A'$ Potential Energy Surfaces," *Journal of Chemical Physics*, Vol. 104, No. 8, 1996, pp. 2825–2833.

[10]Van Driest, E. R., "Turbulent Boundary Layer in Compressible Fluids," *Journal of the Aeronautical Sciences*, Vol. 18, No. 3, 1951, pp. 145–160.

[11]Hopkins, E. J., "Charts for Predicting Turbulent Skin Friction from the Van Driest Method (II)," NASA TN D-6945, Oct. 1972.